Supporting Information

Albantakis and Deco 10.1073/pnas.0901621106

SI Methods

Our model to account for the results from the multiple-choice RDM discrimination experiment of Churchland et al. (1) is based on the network introduced by Brunel and Wang (2). It was originally intended to model object working memory and persistent activity, but was already successfully applied to model neural activity of LIP neurons in the RDM task with two alternatives (3). We extended this neurodynamical framework to decision making with up to 4 alternatives. The competition mechanisms are thereby implemented in the properties of the attractor network, namely high recurrent connectivity and global feedback inhibition. Single neurons are modeled as integrate-and-fire neurons with conductance-based synaptic responses, described by realistic synaptic kinetics.

Experimental Conditions. We tested our model on experimental data from the multiple-choice random-dot motion (RDM) discrimination experiment of Churchland et al. (1). In the RDM task, the subject has to fixate on a central point and is then presented with a number of targets indicating the choice alternatives. One of the targets is located in the response field (RF) of the recorded LIP neuron. After a delay, a patch of dynamic random dots appears with a proportion of dots moving coherently toward one of the targets, while the remaining dots keep moving randomly. The amount of coherence controls the task difficulty. The monkey has to decide on the net direction of motion and report its choice by a saccadic eye movement to the corresponding target. Churchland et al. (1) tested monkeys on the RDM task, comparing 3 different experimental paradigms. Either 2 opposing targets, 4 targets (90° apart) or 2 targets with an angular distance of 90° (90°-case) were presented to the monkey as possible motion directions to decide on.

Network. The network consists of $N_E = 1600$ excitatory pyramidal neurons and $N_I = 400$ inhibitory interneurons, consistent with the neurophysiologically observed proportion of 80% pyramidal cells versus 20% interneurons (4). All simulations were run with a total number of 2,000 neurons. The network is fully connected.

Some of the excitatory neurons are thought to have a selective response to 1 of the 4 targets used in the experiment (1) and, hence, reflect the possible alternatives. Thus, the excitatory neurons are subdivided into 5 populations (pools), the 4 selective pools and a fifth pool of nonselective neurons. The nonselective pool emulates the activity in the surrounding brain areas. Each selective pool contains $f \cdot N_E$ neurons. The fraction f is called the "coding level" of the selective pools. Neuronal pools generally are defined as groups of neurons sharing the same inputs and connectivities. All excitatory neurons are connected to one pool of inhibitory neurons, which regulates the overall activity by implementing competition in the network.

Connectivity Weights. The synaptic efficacies are assumed to be already formed and, therefore, are kept fixed during the simulation. They are consistent with a Hebbian rule: the synapse between 2 cells is strong if their activity was correlated in the past, low if it was anticorrelated. The baseline connection weight between uncorrelated excitatory populations is set to 1. Cells within one selective pool, thus, have stronger weights for recurrent connections ($\omega_+ > 1$), whereas cells between selective pools and from the nonselective to selective pools have weaker connection weights ($\omega < 1$). To model the spatial distribution of the targets in the experiments of Churchland et al. (1), each selective pool in our model is thought to have two "neighboring" selective pools, corresponding to the two targets perpendicular, and one "opposing" pool, representing the target at 180° distance. The connections to and from the neighboring pools are enhanced by a value ω_T, assuming a slightly higher correlation between the neighboring pools than between the anticorrelated opposing pools.

The average excitatory synaptic efficacy should not have changed during the learning process. Therefore, the connections in the network are normalized so that the overall excitatory recurrent synaptic drive remains constant with only baseline input applied to the network (spontaneous state) (2). This is accomplished by adapting ω_- according to

$$\omega_- = 1 - f(2\omega_T + \omega_+ - 1)/(1 - f), \qquad \textbf{[s1]}$$

where f is the coding level. Excitatory-to-inhibitory connections and the mutual connections within the inhibitory pool and the nonselective pool have an intermediate baseline weight of $\omega = 1$. Inhibitory-to-excitatory connections are denoted by a weight ω_I.

Spiking Dynamics. ***Neurons.*** All neurons in the network are modeled as leaky integrate-and-fire (LIF) neurons (5). For the mathematical description of neurons and synapses, we follow the framework of Brunel and Wang (2). Below, we present a summary of the network dynamics. A list of all of the parameters used in our final spiking simulation can be found in Table S1.

LIF neurons are characterized by their subthreshold membrane potential (v) dynamics, given by the equation:

$$C_m \frac{dV(t)}{dt} = -g_m(V(t) - V_L) - I_{syn}(t), \qquad \textbf{[s2]}$$

with a resting potential $V_L = -70$ mV, a membrane capacitance $C_m = 0.5$ nF and a membrane leak conductance $g_m = 25$ nS for pyramidal cells, whereas for interneurons $C_m = 0.2$ nF and $g_m = 20$ nS. I_{syn} is the total synaptic current flowing into the cell. When the membrane potential of a LIF neuron reaches the firing threshold $V_{th} = -50$ mV, a spike is fired and the membrane potential is reset to $V_{reset} = -55$ mV with a refractory period of $\tau_{ref} = 2$ ms for excitatory neurons and $\tau_{ref} = 1$ ms for inhibitory neurons.

Synapses. The neurons in the networks are connected via 3 types of receptors that mediate the synaptic currents flowing into them: AMPA, NMDA glutamate, and $GABA_A$ receptors. The excitatory recurrent postsynaptic currents (EPSCs) are considered to be mediated by fast AMPA ($I_{AMPA,rec}$) and slow NMDA ($I_{NMDA,rec}$) receptors. Neurons, in addition, receive external inputs, representing spontaneous noisy background activity from outside the local network and sensory information processed by other brain areas. These external inputs are assumed to be driven only by AMPA receptors ($I_{AMPA,ext}$). Inhibitory postsynaptic currents (IPSCs) to both excitatory and inhibitory neurons are mediated by $GABA_A$ receptors (I_{GABA}). The total synaptic current is thus given by the sum:

$$I_{syn}(t) = I_{AMPA,rec}(t) + I_{NMDA,rec}(t) + I_{GABA}(t) + I_{AMPA,ext}(t), \quad \textbf{[s3]}$$

The currents are defined by:

$$I_{AMPA,rec}(t) = g_{AMPA,rec}(V(t) - V_E) \sum_{j=1}^{N_E} \omega_j \, s_j^{AMPA,rec}(t) \quad \textbf{[s4]}$$

$$I_{NMDA,rec}(t) = \frac{g_{NMDA}(V(t) - V_E)}{1 + [Mg^{2+}] \exp(-0.062V(t))/3.57} \times \sum_{j=1}^{N_E} \omega_j s_j^{NMDA}(t) \quad \textbf{[s5]}$$

$$I_{GABA}(t) = g_{GABA}(V(t) - V_I) \sum_{j=1}^{N_I} \omega_j s_j^{GABA}(t) \quad \textbf{[s6]}$$

$$I_{AMPA,ext}(t) = g_{AMPA,ext}(V(t) - V_E) \sum_{j=1}^{N_{ext}} s_j^{AMPA,ext}(t), \quad \textbf{[s7]}$$

where $V_E = 0$ mV, $V_I = -70$ mV and ω_j are the synaptic weights. Each receptor has its own fraction s_j of open channels and its own synaptic conductance g. The NMDA synaptic current is potential dependent, controlled by the extracellular concentration of magnesium ($[Mg^{2+}] = 1$ mM) (6).

The neuronal and synaptic capacities and time constants of our model are taken from the original model of persistent activity (2). The conductances there were calibrated to obtain a physiological spontaneous spiking rate of 3 Hz for excitatory neurons and 9 Hz for inhibitory neurons in the unstructured network. As we used 2,000 not 1,000 neurons for all our spiking simulations, the recurrent conductances are scaled by a factor of 1/2 to keep the mean recurrent input constant. In addition, in the model of Brunel and Wang (2), recurrent excitation is largely mediated by NMDA receptors, taking advantage of their slower synaptic dynamics to stabilize the sustained activity state. In our model we could accomplish a better approximation to the experimental findings of Churchland et al. (1) by slightly increasing the amount of AMPA relative to NMDA. Because in the original model the ratio of the NMDA over the AMPA component near firing threshold is 10 in terms of charge entry, a decrease in g_{NMDA} has to be compensated by a 10-fold increase in g_{AMPA} to not change the spontaneous state:

$$g_{NMDA} = g_{NMDA}(1 - \delta), \qquad g_{AMPA} = g_{AMPA}(1 + 10\delta). \quad \textbf{[s8]}$$

Our simulations were run with $\delta = 0.1$, and the recurrent conductances of NMDA and AMPA (both inhibitory and excitatory) were changed according to these rules. Thus, for excitatory neurons $g_{AMPA,ext} = 2.08$ nS, $g_{AMPA,rec} = 0.104$ nS, $g_{NMDA} = 0.14715$ nS and $g_{GABA} = 0.625$ nS; and for inhibitory neurons $g_{AMPA,ext} = 1.62$ nS, $g_{AMPA,rec} = 0.081$ nS, $g_{NMDA} = 0.1161$ nS and $g_{GABA} = 0.4865$ nS. The fraction of open channels or gating variable s_j for AMPA and $GABA_A$ receptor mediated currents is described by:

$$\frac{ds_j(t)}{dt} = -\frac{s_j(t)}{\tau_{decay}} + \sum_k \delta(t - t_j^k), \quad \textbf{[s9]}$$

where the rise time constants have been neglected because they are smaller than 1 ms. This is not possible for NMDA mediated currents with a rise time constant of $\tau_{NMDA,rise} = 2$ ms. There s_j is determined by:

$$\frac{ds_j^{NMDA}(t)}{dt} = -\frac{s_j^{NMDA}(t)}{\tau_{NMDA,decay}} + \alpha x_j(t)(1 - s_j^{NMDA}(t)) \quad \textbf{[s10]}$$

$$\frac{dx_j(t)}{dt} = -\frac{x_j(t)}{\tau_{NMDA,rise}} + \sum_k \delta(t - t_j^k), \quad \textbf{[s11]}$$

with $\alpha = 0.5$ kHz. The sums over k represent a sum over the spike train t_k with δ-Peaks ($\delta(t)$) emitted by presynaptic neuron j at time t_j^k. The values for the decay time constants are $\tau_{AMPA} = 2$ ms for AMPA synapses, $\tau_{NMDA,decay} = 100$ ms for NMDA synapses (7, 8), and $\tau_{GABA} = 10$ ms for GABA synapses (9, 10).

Network Inputs. ***Background activity.*** To simulate spontaneous background activity in the cerebral cortex from outside the local network, all neurons receive an AMPA-mediated external input of uncorrelated Poisson spike trains with a rate of $\nu_{ext} = 2.4$ kHz, equivalent to 800 excitatory connections from external neurons firing at a rate of 3 Hz.

Sensory information. During the random-dot motion experiments of Churchland et al. (1), which we aimed to replicate with our model, the monkeys received 2 sensory stimuli: the target signals and the random-dot motion. One target was always located in the response

field of the recorded neuron. The 4 selective pools in our model are thought to represent the populations of neurons in LIP where the spatial information about one respective target signal and the motion directed toward this target are combined. Therefore, mimicking the experimental protocol, during the spiking simulation an external target and motion input were applied to the network as described below.

Target input. Depending on the number and location of the targets in the different experimental conditions the neurons of either all 4 selective pools, the 2 opposing pools or, in the 90°-case, 2 neighboring pools receive the same target input during the model simulation. We assume that the target input is passed on to the respective pools as a Poisson spike train with a time-dependent firing rate of

$$\nu_{target} = \begin{cases} 0 & 0 < t < t_{\text{target}} \\ (400 + 100\ \exp(-(t - t_{\text{target}})/\tau_1))\ \text{Hz} & t_{\text{target}} \leq t < t_{\text{motion}} + 80\ \text{ms}, \\ (25 + 375\ \exp(-(t - t_{\text{motion}})/\tau_2))\ \text{Hz} & t \geq t_{\text{motion}} + 80\ \text{ms} \end{cases} \quad \textbf{[s12]}$$

where $t_{\text{target}} = 500$ ms and $t_{\text{motion}} = 1300$ ms are the onset times for the target and the motion stimulus, respectively. The time course of the target signal follows the approach of Wong et al. (11) and is in accordance with experimental findings (1, 12). The initial exponential decay, $\tau_1 = 100$ ms, can be explained by short-term adaptation. The "dip" in the firing rate observed immediately after the onset of the motion stimulus is assumed to result from an attentional shift from the targets to the random-dot stimulus or upstream inhibition of the targets with the onset of motion (11, 13). This shift is modeled by an exponential decrease of the target input with $\tau_2 = 15$ ms starting with a latency of 80 ms after motion stimulus onset.

Motion input. During the motion stimulus, LIP neurons are thought to receive inputs from MT neurons depending on the coherence and direction of the random dots. Based on electrophysiological recordings from MT neurons (14, 15), the motion stimulus at zero coherence was simulated in our model as a Poisson spike train with a time invariant rate of motion = 20 Hz to all selective pools. Coherent motion was modeled as a positive bias to one selective pool, balanced by a reduction of the motion input in the other three selective pools, as to keep the total motion input to the network constant. A motion coherence of 100% then corresponds to a bias of 60 Hz to one selective pool, resulting in a motion input of 80 Hz to one and 0 Hz to the other selective pools. As latencies of 200 ms are assumed for the visual information to reach area LIP, the input mimicking the motion stimulus is applied to the selective pools at 1,500 ms. Thus, the there is a gap of 120 ms before the motion input onset where the target input is already decaying, leading to the experimentally observed "dip" in the firing rate.

Simulations. Each trial in the network simulation was run for a total of 4,000 ms. We used a second-order Runge–Kutta routine with a time step of 0.02 ms to perform numerical integration of the coupled differential equations that describe the dynamics of all cells and synapses. The population firing rates were calculated by performing a spike count over a 50-ms window. This sum was then divided by the number of neurons in the population and by the window size. The time window was slided with a time step of 5 ms. A decision was reached when one selective pool crossed a threshold of 50 Hz and surpassed the other selective pools by at least 5 Hz. For each parameter set a block of 1,000 trials with different random seeds was simulated. For the 4-alternative condition in some cases, for small coherence levels, no decision was reached within the 4,000-ms simulation, as all selective pools stayed in the spontaneous state of low firing rate (at most 20 of 1,000 trials). These trials were discarded as failed trials and excluded from the average. In the 90° condition on the other hand, some trials had to be excluded, because the 2 neighboring selective pools stayed in a symmetric double state of enhanced activity and no decision was made (at most 54 of 1,000 trials, for low coherence levels). The mean firing rates and reaction times displayed in Figs. 2 and 3*B* and Fig. S1*B*, S2, and S4 are the average over all trials for the zero coherence case, or else, over all correct trials. In Fig. 3*B* and S1*B* the average population firing rates were grouped into "winning," "losing," and "perpendicular" selective pools. The response time RT was calculated as the difference between the motion onset t_{motion} and the time the threshold was reached t_{thres}, plus an additional time $t_{\text{saccade}} = 80$ ms to account for saccade initiation and execution:

$$\text{RT} = t_{\text{thres}} - t_{\text{motion}} + t_{\text{saccade}}. \quad \textbf{[s13]}$$

Fits to Behavioral Data. The reaction time curve (Fig. 2*A*) was fitted as in Furman and Wang (13) by:

$$\text{RT} = \frac{A}{k \times coh}\ tanh\ (Ak \times coh) + t_{\text{R}}, \quad \textbf{[s14]}$$

with the coherence level *coh* and the free parameters A, k and t_{R}. The psychometric function (Fig. 2*C*) was fitted by a Weibull function:

$$\text{Fraction correct} = (1 - C) \times \exp\ (-(coh/\alpha)^{\beta}), \quad \textbf{[s15]}$$

where C is set as the chance level (0.25 and 0.5 for 2 and 4 choices respectively) and α and β are free parameters.

Mean Field Approximation:. Spiking network simulations are computationally expensive and thus unsuited for systematic parameter explorations. Therefore, we used the mean field approximation derived in Brunel and Wang (2) to scan the parameter space to find a parameter set matching the experimental findings. In addition, the mean-field approximation allowed us to determine conditions where the competition regimes for the 2- and 4-choice cases overlap. This enables decision making between 2 and 4 alternatives with the same set of parameters.

The mean-field approximation provides fixed points of the population firing rates, the stationary states of the populations after the period of dynamical transients. In this formulation the potential of a neuron is calculated as:

$$\tau_x \frac{dV(t)}{dt} = -V(t) + \mu_x + \sigma_x\ \sqrt{\tau_x}\eta(t), \quad \textbf{[s16]}$$

where $V(t)$ is the membrane potential, x labels the populations, τ_x is the effective membrane time constant, μ_x is the mean value the membrane potential would have in the absence of spiking and fluctuations, σ_x measures the magnitude of the fluctuations and η is a Gaussian process with absolute exponentially decaying correlation function and time constant τ_{AMPA}. The quantities μ_x and σ_x^2 are given by:

$$\mu_x = \frac{(T_{\mathrm{ext}}\nu_{\mathrm{ext}} + T_{\mathrm{AMPA}}n_x^{\mathrm{AMPA}} + \rho_1 n_x^{\mathrm{NMDA}})V_{\mathrm{E}} + \rho_2 n_x^{\mathrm{NMDA}}\langle V\rangle + T_{\mathrm{I}}n_x^{\mathrm{GABA}}V_{\mathrm{I}} + V_{\mathrm{L}}}{S_{\mathrm{x}}} \quad \textbf{[s17]}$$

$$\sigma_x^2 = \frac{g_{\mathrm{AMPA,ext}}^2(\langle V\rangle - V_{\mathrm{E}})^2 N_{\mathrm{ext}}\nu_{\mathrm{ext}}\tau_{\mathrm{AMPA}}^2\tau_x}{g_{\mathrm{m}}^2\tau_{\mathrm{m}}^2}. \quad \textbf{[s18]}$$

where ν_{ext} is the external incoming spiking rate, ν_{I} is the spiking rate of the inhibitory population, $\tau_{\mathrm{m}} = C_{\mathrm{m}}/g_{\mathrm{m}}$ with the values for the excitatory or inhibitory neurons depending of the population considered. The other quantities are given by:

$$S_x = 1 + T_{\mathrm{ext}}\nu_{\mathrm{ext}} + T_{\mathrm{AMPA}}n_x^{\mathrm{AMPA}} + (\rho_1 + \rho_2)n_x^{\mathrm{NMDA}} + T_{\mathrm{I}}n_x^{\mathrm{GABA}} \quad \textbf{[s19]}$$

$$\tau_x = \frac{C_{\mathrm{m}}}{g_{\mathrm{m}}S_x} \quad \textbf{[s20]}$$

$$n_x^{\mathrm{AMPA}} = \sum_{j=1}^{p} f_j\omega_{jx}^{\mathrm{AMPA}}\nu_j \quad \textbf{[s21]}$$

$$n_x^{\mathrm{NMDA}} = \sum_{j=1}^{p} f_j\omega_{jx}^{\mathrm{NMDA}}\psi(\nu_j) \quad \textbf{[s22]}$$

$$n_x^{\mathrm{GABA}} = \sum_{j=1}^{p} f_j\omega_{jx}^{\mathrm{GABA}}\nu_j \quad \textbf{[s23]}$$

$$\psi(\nu) = \frac{\nu\tau_{\mathrm{NMDA}}}{1 + \nu\tau_{\mathrm{NMDA}}}\left(1 + \frac{1}{1 + \nu\tau_{\mathrm{NMDA}}}\sum_{n=1}^{\infty}\frac{(-\alpha\tau_{\mathrm{NMDA,rise}})^n T_n(\nu)}{(n+1)!}\right) \quad \textbf{[s24]}$$

$$T_n(\nu) = \sum_{j=1}^{n}(-1)^k\binom{n}{k}\frac{\tau_{\mathrm{NMDA,rise}}(1 + \nu\tau_{\mathrm{NMDA}})}{\tau_{\mathrm{NMDA,rise}}(1 + \nu\tau_{\mathrm{NMDA}}) + k\tau_{\mathrm{NMDA,decay}}} \quad \textbf{[s25]}$$

$$\tau_{\mathrm{NMDA}} = \alpha\tau_{\mathrm{NMDA,rise}}\tau_{\mathrm{NMDA,decay}} \quad \textbf{[s26]}$$

$$T_{\mathrm{ext}} = \frac{g_{\mathrm{AMPA,ext}}\tau_{\mathrm{AMPA}}}{g_{\mathrm{m}}} \quad \textbf{[s27]}$$

$$T_{\mathrm{AMPA}} = \frac{g_{\mathrm{AMPA,rec}}N_{\mathrm{E}}\tau_{\mathrm{AMPA}}}{g_{\mathrm{m}}} \quad \textbf{[s28]}$$

$$\rho_1 = \frac{g_{\mathrm{NMDA}}N_{\mathrm{E}}}{g_{\mathrm{m}}J} \quad \textbf{[s29]}$$

$$\rho_2 = \beta\frac{g_{\mathrm{NMDA}}N_{\mathrm{E}}(\langle V_x\rangle - V_{\mathrm{E}})(J-1)}{g_{\mathrm{m}}J^2} \quad \textbf{[s30]}$$

$$J = 1 + \gamma\exp(-\beta\langle V_x\rangle) \quad \textbf{[s31]}$$

$$T_1 = \frac{g_{\mathrm{GABA}}N_1\tau_{\mathrm{GABA}}}{g_{\mathrm{m}}} \quad \textbf{[s32]}$$

$$\langle V_x\rangle = \mu_x - (V_{\mathrm{thr}} - V_{\mathrm{reset}})\nu_x\tau_x, \quad \textbf{[s33]}$$

where p is the number of excitatory populations, f_x is the fraction of neurons in the excitatory population x, $\omega_{j,x}$ the weight of the connections from population x to population j, ν_x is the spiking rate of the excitatory population x, $\gamma = [\mathrm{Mg}^{2+}]/3.57$, $\beta = 0.062$ and the average membrane potential $\langle V_x\rangle$ has a value between -55 mV and -50 mV.

The mean-field approximation finally yields a set of n nonlinear equations describing the average firing rates of the different populations in the network as a function of the defined quantities μ_x and σ_x:

$$\nu_x = \phi(\mu_x, \sigma_x), \qquad x = 1, \ldots, n, \tag{s34}$$

where ϕ is the transduction function of population x, which gives the output rate of a population x in terms of the inputs, which in turn depend on the rates of all of the populations.

$$\phi(\mu_x, \sigma_x) = \left(\tau_{rp} + \tau_x \int_{\beta(\mu_x,\sigma_x)}^{\alpha(\mu_x,\sigma_x)} du \sqrt{\pi} \exp(\mu^2)[1 + \mathrm{erf}(u)] \right)^{-1} \tag{s35}$$

$$\alpha(\mu_x, \sigma_x) = \frac{(V_{\mathrm{thr}} - \mu_x)}{\sigma_x} \left(1 + 0.5 \frac{\tau_{\mathrm{AMPA}}}{\tau_x} \right) + 1.03 \sqrt{\frac{\tau_{\mathrm{AMPA}}}{\tau_x}} - 0.5 \frac{\tau_{\mathrm{AMPA}}}{\tau_x} \tag{s36}$$

$$\beta(\mu_x, \sigma_x) = \frac{(V_{\mathrm{reset}} - \mu_x)}{\sigma_x} \tag{s37}$$

with $\mathrm{erf}(u)$ the error function and τ_{rp} the refractory period which is considered to be 2 ms for excitatory neurons and 1 ms for inhibitory neurons. To solve the equations defined by Eq. **s34** for all x we numerically integrate Eq. **s33** and the differential equation below, whose fixed-point solutions correspond to solutions to Eq. **s34**:

$$\tau_x \frac{d\nu_x}{dt} = -\nu_x + \phi(\mu_x, \sigma_x). \tag{s38}$$

For the numerical integration, we used an Euler routine with a step size of 0.1 ms. To find all of the possible fixed points that coexist for a given parameter set, we integrated Eq. **s38** with different initial conditions of population firing rates. We used 4 initial conditions spanning the possible firing rates at different temporal stages of the spiking simulation and the different experimental conditions:

1. all selective pools with an initial firing rate of 0 Hz,
2. 1 selective pool 120 Hz, the other 3 pools 0 Hz,
3. 2 opposing selective pools 30 Hz, the other 2 0 Hz,
4. all selective pools with 30 Hz.

For our modeling purpose, decision making between 2 and 4 alternatives, we intended to find a region of multistability with competition, so that always just 1 selective pool would terminate in an up-state of high firing rate. For specific sets of model parameters, the stable fixed points were calculated over a range of external inputs from 0 to 100 Hz in steps of 0.5 Hz for the 2- and 4-choice condition (Fig. 4*A*). The range of external inputs where for all initial conditions and both experimental paradigms a decision is reached, i.e., 1 and just 1 pool is in an up-state, was termed "range of decision making." Keeping the other parameters fixed, the value of the neighboring connectivity ω_{T} with the optimal, i.e., broadest, range of decision making was determined by performing the fixed-point analysis explained above for $\omega_{\mathrm{T}} = 0 \ldots 0.1$ with steps of 0.0025 (Fig. 4*B*). To explore the relation between the coding level f and the range of decision making, the optimal value of ω_{T} was determined for 11 different values of f from 0.1 to 0.225. When changing the coding level, the network connectivities have to be adapted (Fig. 4*C*) to keep the up-state fixed-point firing rates at the same values. Thus, the connectivity ω_+ was adjusted in steps of 0.0025 until the up-state fixed points matched the values for the parameters of the spiking simulation ($f = 0.2$ and $\omega_+ = 1.48$) (Fig. 4*A*). Note, that with changing ω_+ also ω_- changes, because of the normalization condition Eq. S1. For the final values of ω_+ for the respective coding levels, the up-state fixed-point values deviated by less than 2 Hz in the range of external inputs from 20 to 60 Hz. The optimal range of decision making was plotted against the coding level and fitted by a linear function (Fig. 4*D*).

Parameters. See Table S1 for the default parameter set used in the integrate-and-fire simulation.

1. Churchland AK, Kiani R, Shadlen MN (2008) Decision-making with multiple alternatives. *Nat Neurosci* 11(6):693–702.
2. Brunel N, Wang XJ (2001) Effects of neuromodulation in a cortical network model of object working memory dominated by recurrent inhibition. *J Comput Neurosci* 11(1):63–85.
3. Wang XJ (2002) Probabilistic decision making by slow reverberation in cortical circuits. *Neuron* 36:955–968.
4. Abeles M (1991) *Corticonics: Neural Circuits of the Cerebral Cortex* (Cambridge Univ Press, Cambridge, UK).
5. Tuckwell H (1988) *Introduction to Theoretical Neurobiology* (Cambridge Univ Press, Cambridge, UK).
6. Jahr C, Stevens C (1990) Voltage dependence of NMDA-activated macroscopic conductances predicted by single-channel kinetics. *J Neurosci* 10(9):3178–3182.
7. Hestrin S, Sah P, Nicoll R (1990) Mechanisms generating the time course of dual component excitatory synaptic currents recorded in hippocampal slices. *Neuron* 5(3):247–53.
8. Spruston N, Jonas P, Sakmann B (1995) Dendritic glutamate receptor channels in rat hippocampal CA3 and CA1 pyramidal neurons. *J Physiol* 482(2):325–352.
9. Salin P, Prince D (1996) Spontaneous GABAA receptor-mediated inhibitory currents in adult rat somatosensory cortex. *J Neurophysiol* 75(4):1573–1588.
10. Xiang Z, Huguenard J, Prince D (1998) GABAA receptor-mediated currents in interneurons and pyramidal cells of rat visual cortex. *J Physiol* 506(3):715–730.
11. Wong KF, Huk AC, Shadlen MN, Wang XJ (2007) Neural circuit dynamics underlying accumulation of time-varying evidence during perceptual decision making. *Front Comput Neurosci* 1:6.
12. Huk AC, Shadlen MN (2005) Neural activity in macaque parietal cortex reflects temporal integration of visual motion signals during perceptual decision making. *J Neurosci* 25(45):10420.
13. Furman M, Wang XJ (2008) Similarity effect and optimal control of multiple-choice decision making. *Neuron* 60(6):1153–1168.
14. Britten KH, Shadlen MN, Newsome WT, Movshon JA (1993) Responses of neurons in macaque MT to stochastic motion signals. *Vis Neurosci* 10(6):1157–1169.
15. Britten KH, Newsome WT (1998) Tuning bandwidths for near-threshold stimuli in area MT. *J Neurophysiol* 80(2):762–770.

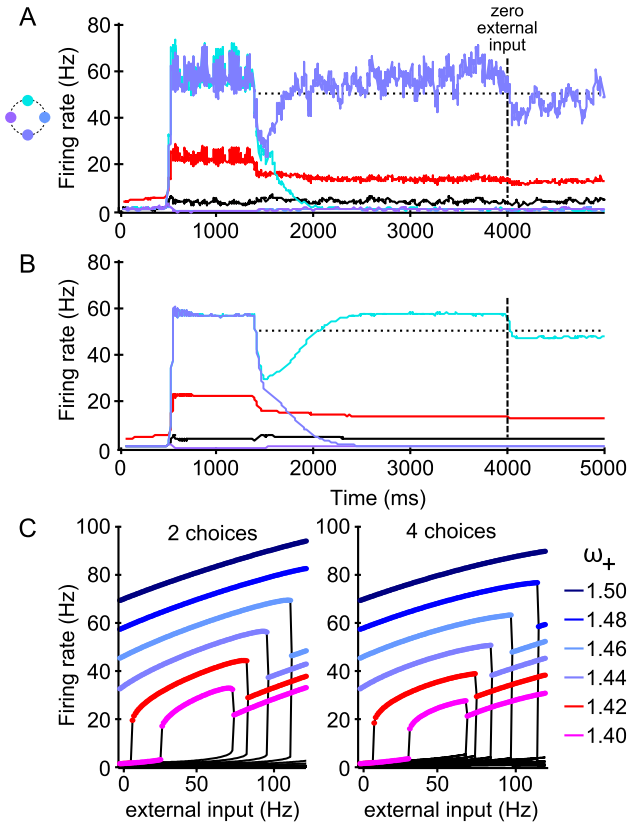

Fig. S1. Network exhibits persistent activity after the external inputs are switched off. (*A* and *B*) Displayed are a single trial (*A*) and the trial average over 1,000 network simulations (*B*) at zero motion coherence for the 2-choice case (colors as in Fig. 3, main text, red and black lines denote inhibitory and nonselective pools). The time course of the external inputs is the same as shown in Fig. 1*D*, until at 4,000 ms, all external inputs are switched off. The selective population that ''won'' the competition sustains its activity at about 48 Hz in all trials. (*C*) The attractor state is persistent due to the strong recurrent connectivity. Shown are the stable attractor states of the network calculated in the mean-field approximation (see *SI Text*) for different values of the recurrent connectivity ω_+. The initial condition was: 1 pool initialized at 120 Hz, the other 3 pools at 0 Hz, which corresponds to the situation when 1 pool has already ''won'' the decision. For $\omega_+ > 1.44$, the decision state exists and is stable even for zero external input. For smaller values of ω_+, a decision state with high firing rates occurs only at higher external inputs. In our simulations, we use $\omega_+ = 1.48$ and, therefore, reliably obtain persistent activity with our network.

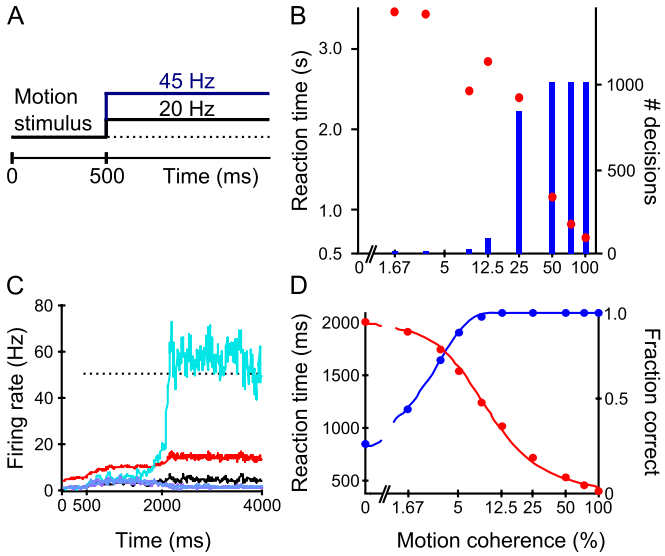

Fig. S2. Network simulations without target stimulus. (*A*) Time course of the external input. To investigate the network's behavior without the target input, we performed 2 sets of simulations, 1 with a motion signal of 20 Hz and 1 with 45 Hz applied to the 4 selective pools. (*B*) For the 20-Hz motion signal for small coherence levels (until 12.5%), the input to the selective populations is too low to induce a decision. The number of decisions is shown by the blue bars (right ordinate). In most of the trials with small coherences, all pools stay in their spontaneous states (see also Fig. 4*A*, main text: The black line represents the mean-field initial condition where all pools start at 0 Hz. For 20-Hz external input, the network stays in its spontaneous state). However, for higher coherence levels, the model is capable of reaching a decision in nearly all cases, with realistic reaction times (red dots, left ordinate). At these high coherence levels, the network only takes correct decisions. (*C*) Single trial at 0% coherence for a motion signal of 45 Hz. The integration process starts at 500 ms, a decision is reached at ≈2,000 ms. (*D*) Speed and accuracy of the 45-Hz simulations. Red (left ordinate): reaction times of correct trials as a function of motion coherence, fitted by a hyperbolic tangent function (see *SI Text*). For lower coherences, decisions take longer than with the target signal (Fig. 2 *A*, main text). This is very realistic, because the random-dot motion task is more difficult without knowledge about the possible targets. Blue (right ordinate): Psychometric function, fitted by a Weibull function (see *SI Text*). Accuracy starts at chance level, as with the target signal, and reaches 100% for higher coherence levels. One thousand trials were simulated for each data point. At low motion coherence, at most 4% of the trials had to be excluded, because they failed to reach a decision within the simulation time of 4,000 ms. Our simulations show that for a strong enough motion signal, our network is capable of decision making without the target signal. This corresponds to possible experiments where subjects have to decide on the direction of coherent motion without previously being shown any target possibilities. However, it must be noted that our model is restricted to its 4 selective populations. To model continuous decision making, a higher number of pools would be needed (see *Discussion*, main text).

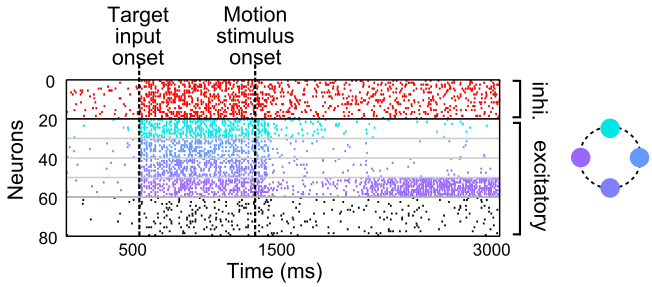

Fig. S3. Spike raster plot of simulated neural activity for sample neurons of each network pool in a 4-choice trial with zero motion coherence. Shown is the same trial as in Fig. 3*B Middle*. Displayed are 20 inhibitory neurons (red, top row), 20 nonselective neurons (black, bottom row), and 10 neurons of each selective pool, colored according to the schematic illustration of target location (right). All selective neurons (21 to 60) receive the same input, because the motion coherence is zero. Nevertheless, the network exhibits competition due to its stochastic dynamics. Eventually (at ≈2,000 ms) the symmetry is broken, and, in this case, the activity of the left pool (purple) shifts to an attractor state with increased activity (up-state).

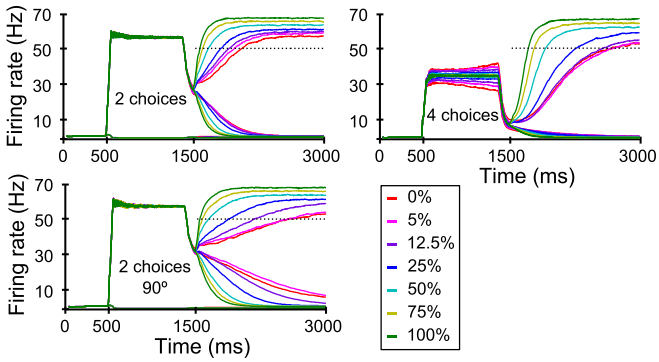

Fig. S4. Population-averaged temporal evolution of firing rates at different motion strengths for the 3 tested conditions. The average of the correct trials of each motion coherence level is shown for the 3 different experimental conditions. Different colors denote different motion coherence (see legend). The build-up rate increases with increasing motion coherence in all cases, as observed experimentally in LIP neurons. This explains the faster reaction times for increasing motion coherence.

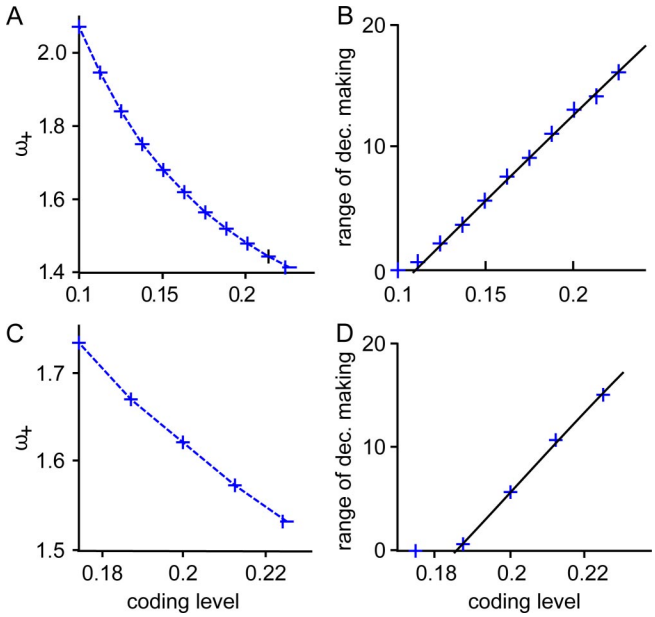

Fig. S5. Range of decision making for smaller AMPA/NMDA ratio. A linear relation between the range of decision making and the coding level was also found for the original AMPA/NMDA ratio used in the model of Brunel and Wang (1) (*SI Methods*), Eq. **S8** $\delta = 0$). We tested 2 conditions: (*i*) (*A*, *B*) All network parameters are the same as in Fig. 4, except for a smaller AMPA/NMDA ratio. In this case, the up-state fixed-point firing rates are lower than the firing rates found in the experiments. (*A*) The connectivity ω_+ was adapted as in Fig. 4*C*, so that the up-states deviated by less than 2 Hz from the up-state value at $\omega_+ = 1.48$ (value used in the spiking simulations). (*B*) The optimal range of decision making (see Fig. 4*D*) still increases linearly with the coding level. (*ii*) (*C*, *D*) The connectivity ω_+ was adapted with the AMPA/NMDA ratio, so that firing rates are in the same range as in the spiking simulations and experiments. The range of decision making again increased linearly with the coding level. However, due to the higher ω_+ values (*C*), the optimal range of decision making resulting was much smaller, and already for a coding level of 0.175, no common decision state could be found for the 2- and 4-choice task.

1. Brunel N, Wang XJ (2001) Effects of neuromodulation in a cortical network model of object working memory dominated by recurrent inhibition. *J Comput Neursci* 11(1):63–85.

Table S1. The default parameter set used in the integrate-and-fire simulation

Parameter	Value
N_E	1,600
N_I	400
N_{ext}	800
ν_{ext}	2.4 kHz
f	0.20
ω_+	1.48
ω_I	1.125
ω_T	0.015
C_m (excitatory)	0.5 nF
C_m (inhibitory)	0.2 nF
g_m (excitatory)	25 nS
g_m (inhibitory)	20 nS
τ_{ref} (excitatory)	2 ms
τ_{ref} (inhibitory)	1 ms
V_E	0 mV
V_I	−70 mV
V_L	−70 mV
V_{thr}	−50 mV
V_{reset}	−55 mV
$g_{AMPA,ext}$ (excitatory)	2.08 nS
$g_{AMPA,rec}$ (excitatory)	0.104 nS
g_{NMDA} (excitatory)	0.14715 nS
g_{GABA} (excitatory)	0.625 nS
$g_{AMPA,ext}$ (inhibitory)	1.62 nS
$g_{AMPA,rec}$ (inhibitory)	0.081 nS
g_{NMDA} (inhibitory)	0.1161 nS
g_{GABA} (inhibitory)	0.4865 nS
$\tau_{NMDA,decay}$	100 ms
$\tau_{NMDA,rise}$	2 ms
τ_{AMPA}	2 ms
τ_{GABA}	10 ms
a	0.5 ms^{-1}